PLASMA DYNAMICS

VIII. PLASMA PHYSICS[*]

Prof. S. C. Brown
Prof. G. Bekefi
Prof. K. U. Ingard
Prof. D. R. Whitehouse
Dr. J. C. Ingraham
M. L. Andrews
V. Arunasalam
C. D. Buntschuh
J. D. Coccoli

F. X. Crist
J. K. Domen
E. W. Fitzgerald, Jr.
D. L. Flannery
G. A. Garosi
K. W. Gentle
W. H. Glenn, Jr.
E. B. Hooper, Jr.
P. W. Jameson
R. L. Kronquist

J. J. Linehan
D. T. Llewellyn-Jones
E. M. Mattison
J. J. McCarthy
W. J. Mulligan
J. J. Nolan, Jr.
G. L. Rogoff
F. Y-F. Tse
B. L. Wright

A. FURTHER OBSERVATIONS OF ANOMALOUS CYCLOTRON RADIATION IN XENON AND KRYPTON

We have continued the investigation into the nature of the anomalous cyclotron emission emanating from the cathode region of discharges in gases possessing a pronounced Ramsauer effect. This radiation was first observed by Tanaka, Mitani, and Kubo[1] in xenon and krypton. They suggested that the radiation was a manifestation of the negative absorption predicted by Bekefi, Hirshfield, and Brown[2] and by Twiss.[3]

Many additional details of this radiation were reported by Coccoli.[4] It was observed that the radiation was pulsed, and that it was possible to trigger these pulses synchronously with relaxation oscillations of the plasma. The pulses were of microsecond duration and spaced on the average at millisecond intervals. Therefore, the pulse amplitude was found to be several orders of magnitude greater than the average measured by Tanaka et al.[1] with a radiometer. It was further observed that the amplitude of these pulses was sensitive to the orientation of the discharge tube with respect to the external magnetic field. The largest amplitudes were found when the discharge tube axis was oriented at an angle to the magnetic field. The tentative explanation was offered that the transverse component of the electron energy increased at nonparallel alignment,
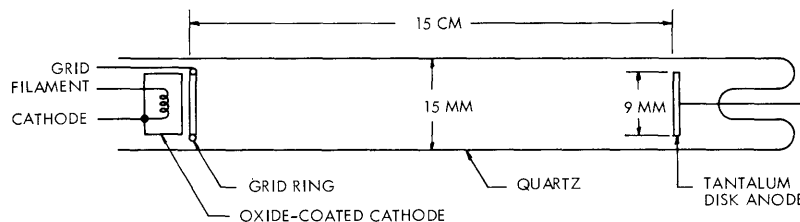

Fig. VIII-1. Discharge tube. The grid ring distorts electric field near cathode, providing control over the transverse component of the electron velocity.

MAGNETIC FIELD (GAUSS)
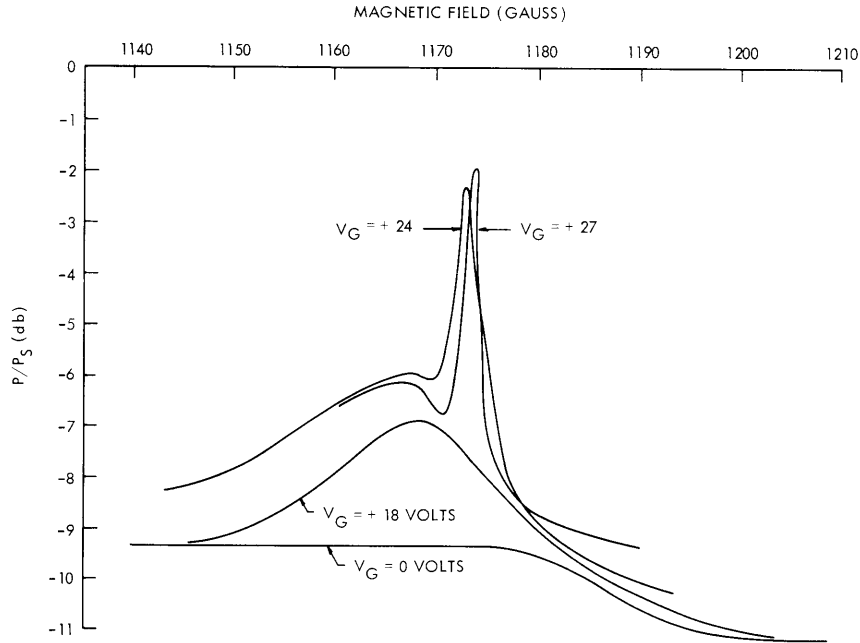

Fig. VIII-2.   Radiometer measurement of xenon cyclotron
plasma emission at various grid voltages.

I_d = 71 ma

p = 830 μ Hg.

since the transverse component of the DC electric field in the cathode region would vary with tube orientation. It was also observed that the maximum power radiated in the anomalous cyclotron mode occurred at a gas pressure of slightly more than 1 mm Hg in xenon. These results were obtained by using a cathode similar in design to that described by Tanaka et al.[1]

The tentative explanation of the variation of the anomalous cyclotron radiation intensity with orientation of the discharge tube suggested the construction of the new discharge tube shown in Fig. VIII-1. The cathode surface is a flat circular oxide-coated nickel disc whose normal is parallel to the axis of the discharge tube. A tungsten ring with an inner diameter equal to the diameter of the cathode was placed 2 mm above the cathode surface. When a voltage is applied to the grid ring, it distorts the electric field in the cathode region. The transverse velocity component of the electrons increases as the grid is made more positive with respect to the cathode. Figure VIII-2 shows the effect of increasing the transverse component of the electron velocity on the amplitudes of the normal and anomalous cyclotron radiations from a xenon discharge. With no voltage difference between the cathode and grid ring, the plasma emission at a fixed microwave frequency, ω_o, is almost independent of magnetic field below the cyclotron frequency and decreases slightly because of an increased reflection coefficient above the cyclotron
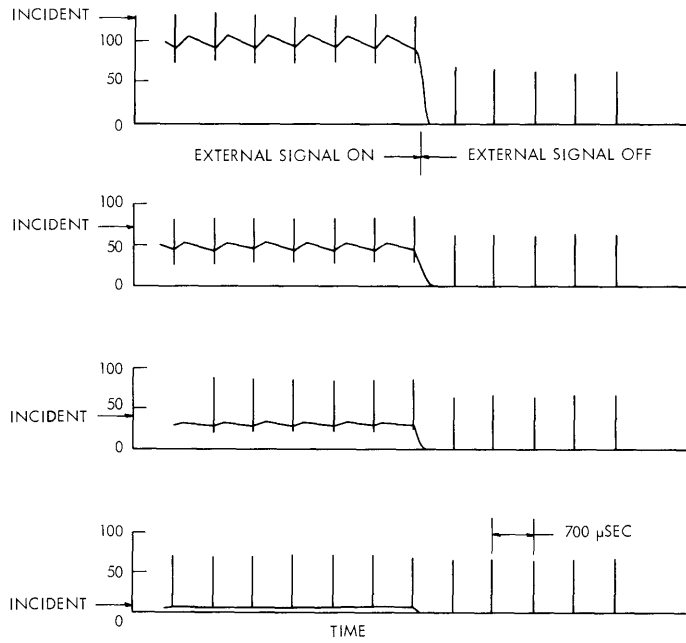
Fig. VIII-3. Anomalous cyclotron emission and absorption pulses at various external signal levels. $p = 500 \mu$ Hg, $I_d = 25$ ma, $\omega = \omega_b$, tube diameter, 15 mm.
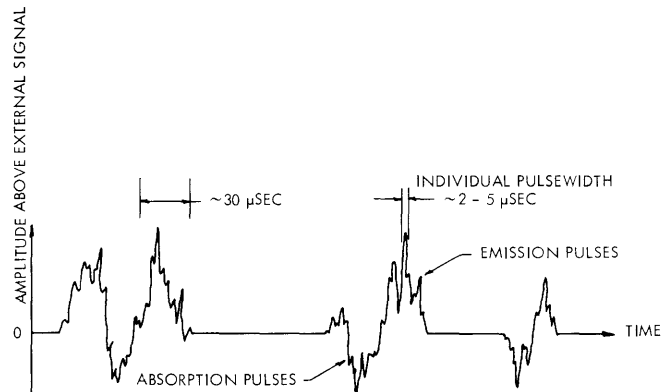

Fig. VIII-4. Detail of anomalous cyclotron emission and absorption pulses and pulse clusters.

frequency. As the grid is made more positive with respect to the cathode, the normal cyclotron emission line appears and increases, which is a good indication that the transverse component of the electron velocity is increasing. At a certain value of the grid-to-cathode potential, the narrow anomalous cyclotron line appears. The measurements shown in Fig. VIII-2 were taken with a radiometer and therefore represent an average rate of radiation at each value of magnetic field. The amplitude of the individual pulses of anomalous cyclotron radiation are 20 db or more greater than the average.

When an external signal whose amplitude is comparable with or greater than that of the anomalous radiation pulses is incident on the plasma, the transmitted signal exhibits an anomalous cyclotron absorption[4] (Fig. VIII-3). Both emission and absorption pulses occurred simultaneously within the limit of resolution of the observations in Fig. VIII-3. We were able to resolve the pulse patterns, and these are sketched from oscillographs and shown in Fig. VIII-4. The pulses in Fig. VIII-4 were obtained from a krypton discharge at a pressure of 1 mm Hg. Under these conditions, the pulses occurred in random groups of twenty or thirty pulses per group. No particular order of occurrence of the emission and absorption pulses was evident. However, absorption pulses were never found separated by more than a pulse width from emission pulses.

Figure VIII-5 shows the amplitude of the pulses of anomalous cyclotron emission as a function of gas pressure in krypton when all of the conditions, such as discharge current, magnetic field, and grid voltage, have been adjusted for maximum pulse height. Also shown in Fig. VIII-5 is the frequency of occurrence of the pulses as a function of gas pressure when conditions were adjusted for maximum pulse height. The average power radiated is proportional to the product of the two curves, and is a maximum at approximately 1.2 mm Hg. This is nearly the same value found in xenon.[4]

It was observed that as the frequency of occurrence of the pulses increased, the pulses tend to cluster in groups of increasing population, rather than occurring as single, widely separated random events. At a frequency of occurrence of a few thousand per second or less, the pulses appear singly or doubly. At a frequency of occurrence of 100,000 per second, the pulses overlap in clusters of twenty, thirty or more. When there is a large amount of pulse overlap, the electronic counter does not resolve every pulse. This probably accounts for the flat portion in the curve of pulse frequency versus gas pressure in Fig. VIII-5. The maximum pulse rate is probably in excess of 150,000/sec at a pressure of 1000 μ Hg.

These experiments were repeated with helium. Helium does not contain a Ramsauer minimum in its electron collision cross section. The anomalous cyclotron emission and absorption were not detected.

These experiments were repeated with neon. Neon has a small collision cross section (relative to xenon, argon, and krypton) over the range of electron energy of interest. Neon has a shallow Ramsauer slope that does not satisfy one of the theoretical conditions
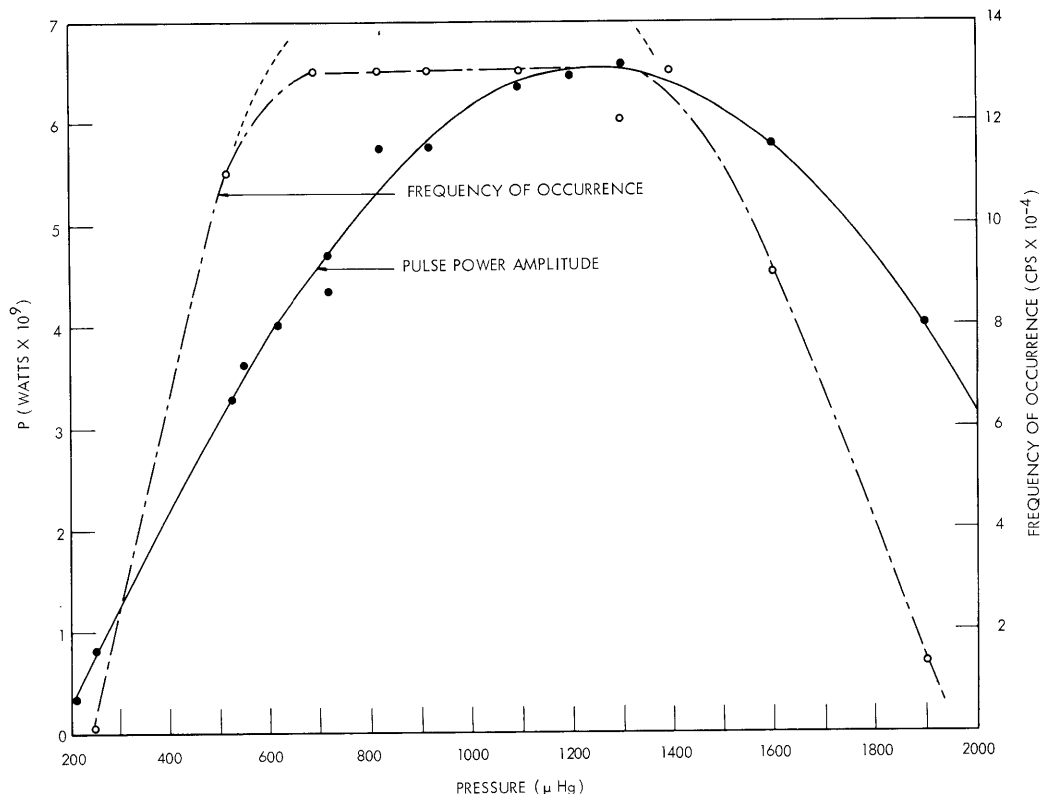
Fig. VIII-5. Amplitude and frequency of occurrence of anomalous cyclotron emission pulses in krypton as a function of gas pressure.

needed for gain. The anomalous cyclotron absorption and emission were not detected experimentally in neon.

Argon has a pronounced Ramsauer minimum in its electron collision cross section. By a process of curve fitting, however, we do not find the negative slope of the collision cross section versus electron energy curve satisfying the gain condition (or at best, marginal over a limited portion of the curve). The anomalous cyclotron emission and absorption were not detected experimentally in argon by us.

Tanaka et al.[1] claim to have seen the anomalous cyclotron emission in xenon, krypton, and argon, and present data for xenon and krypton but not for argon. If the effect exists in argon, it is probably much smaller than in xenon and quite sensitive to the electron energy distribution.

It seems very probably from the large amount of power radiated in the anomalous cyclotron pulses in xenon and krypton and the lack of pulses in helium, neon and thus far argon that the explanation is the negative absorption mechanism. Because of the geometry involved, however, attempts to couple external signals to the small region of emission near the cathode have not yet succeeded. The absorption data taken thus

far have only displayed a positive anomalous absorption. Attempts to amplify an external signal will be continued.

J. D. Coccoli

References

1. S. Tanaka, K. Mitani, and H. Kubo, Experiments on the Negative Radiation Temperature at Cyclotron Resonance in Cold Plasmas, Research Report IPPJ-6, Institute of Plasma Physics, Nagoya University, February 1963.

2. G. Bekefi, J. Hirshfield, and S. C. Brown, Phys. Fluids 4, 173 (1961); Phys. Rev. 122, 1037 (1961).

3. R. Q. Twiss, Australian J. Phys. 11, 564 (1958).

4. J. D. Coccoli, Anomalous pulsed emission and absorption by a xenon plasma at the electron-cyclotron frequency, Quarterly Progress Report No. 72, Research Laboratory of Electronics, M. I. T., January 15, 1964, pp. 102-111.

B. ION CONFINEMENT WITH STATIC AND ROTATING B FIELDS

Electromagnetic fields have long been proposed for particle and plasma confinement. Most schemes involve the use of radiation fields in which the force is related to the gradient in the energy density of the field. Recently, Insinger et al.[1] have studied particle orbits in independent, quasi-static electric and magnetic fields. They indicate the general solution for E and B fields rotating in a plane perpendicular to a static B field. Blevin and Thonemann[2] used this geometry to generate radial compression of a plasma column.

Our interest in this problem stems from the desire to produce quiescent low-density plasmas at very low pressures. Jameson[3] has reported on some calculations of particle confinement with a microwave cavity at electron-cyclotron resonance. This report concerns an alternative approach of axial confinement of ions in a uniform magnetic field as shown in Fig. VIII-6 with the use of rotating magnetic fields at the ion-cyclotron frequency. The advantages of such a scheme are (i) there is selective ion confinement,
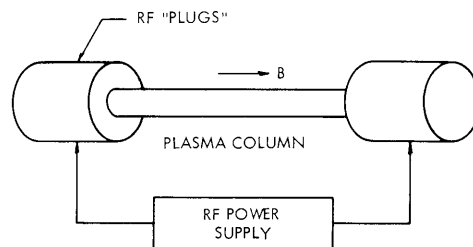

Fig. VIII-6. Confinement scheme.

(ii) the frequencies are low and the RF B field is not distorted except for very high den-sity plasmas, and (iii) the reflection occurs essentially adiabatically in that the ions transfer very little energy with the field. In order to analyze the interaction, we show the disposition of the fields of the "RF plug" in Fig. VIII-7. A single-turn coil or shorted
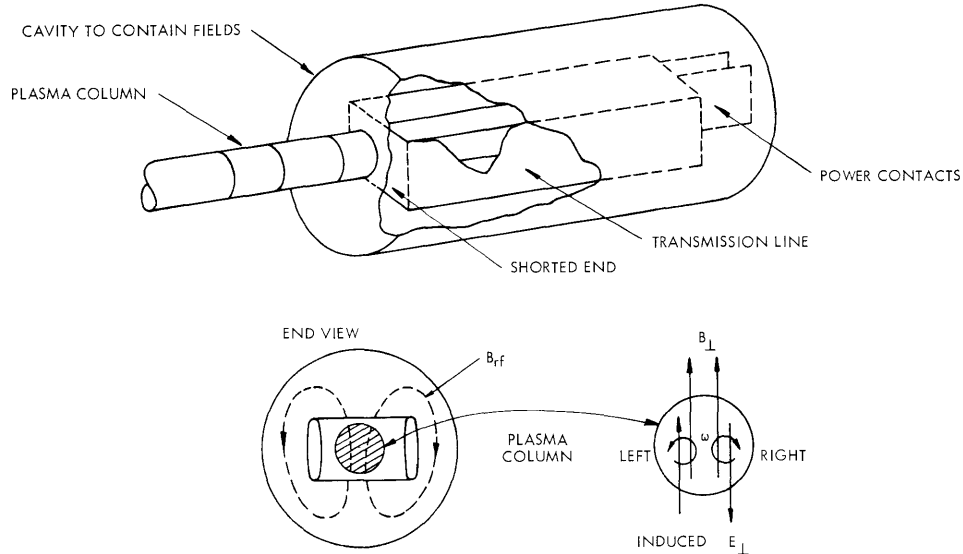

Fig. VIII-7. One phase of rotating field in RF plug.

transmission line is mounted inside a cylindrical shield such that the field in the x-y plane is dipolar and approximately uniform over the cross section of the plasma. Another transmission line (not shown) is aligned perpendicular to the first and produces a B field in the y direction such that the total B either rotates left- or right-handed around the z axis. The first-order induced electric field for this geometry is either parallel or antiparallel to the RF B and increases in magnitude proportional to z. These fields are uniform except at the entrance of the plasma into the cavity where some fringing will occur. The field configuration differs from that of Insinger et al.[1] in that the induced E is along $B_\perp$ rather than in the z direction.

To a good approximation, the fields in the interaction region (z > 0) are given by

$$\overline{B} = (\hat{x} \mp j\hat{y})B_\perp \, e^{j\omega t} + \hat{z}B_z \tag{1}$$

$$\overline{E} = \mp(\hat{x} \mp j\hat{y})z\omega B_\perp \, e^{j\omega t}, \tag{2}$$

where the upper and lower signs indicate rotating fields, right- and left-handed, respectively, and the E field was obtained to first order from $\overline{\nabla} \times \overline{E} = -\dot{\overline{B}}$ and the

appropriate boundary conditions.

Define

$$\Omega_{\perp} = -\frac{qB_{\perp}}{m}, \qquad \Omega_{z} = -\frac{qB_{z}}{m}.$$ (3)

The equation of motion, $m\ddot{\bar{r}} = q(\overline{E} + \dot{\bar{r}} \times \overline{B})$ now gives for the three components,

$$\ddot{x} = \pm z\omega\Omega_{\perp}\cos\omega t \pm \dot{z}\Omega_{\perp}\sin\omega t - \dot{y}\Omega_{z}$$ (4)

$$\ddot{y} = +z\omega\Omega_{\perp}\sin\omega t - \dot{z}\Omega_{\perp}\cos\omega t + \dot{x}\Omega_{z}$$ (5)

$$\ddot{z} = \mp\dot{x}\Omega_{\perp}\sin\omega t + \dot{y}\Omega_{\perp}\cos\omega t.$$ (6)

If we differentiate Eq. 6, substitute from Eqs. 4 and 5, differentiate again, substitute again from Eqs. 4 and 5, and then combine the result with Eq. 6, we obtain a fourth-order differential equation for z with constant coefficients.

$$\ddddot{z} + \left[\Omega_{\perp}^{2} + (\omega \mp \Omega_{z})^{2}\right]\ddot{z} + \omega(\omega \mp \Omega_{z})\Omega_{\perp}^{2}z = 0$$ (7)

The presence of the last term is a result of the induced electric field. In solving for $z(t)$, the four constants of integration are determined from $z(0)$, $\dot{z}(0)$, $\dot{x}(0)$, and $\dot{y}(0)$. The solution is independent of $x(0)$ and $y(0)$, since the field pattern is independent of x and y.

We now specialize the solution for ion-cyclotron resonance so that we have the left-handed rotation and $\omega + \Omega_{z} = 0$. Equation 7 becomes

$$\ddddot{z} + \Omega_{\perp}^{2}\ddot{z} = 0,$$ (8)

where the last term of (7) drops out, thereby indicating that the z motion is independent of E. This fact is consistent, since at resonance the velocity caused by $\overline{E}$ will be aligned with $\overline{E}$, which in turn is aligned with $B_{\perp}$, and this only interacts with B_{z}, giving a perpendicular force.

Let the particle enter the cavity at $t = 0$, where with no loss of generality $B_{\perp}$ is in the x direction. The initial conditions are thus

$$z(0) = 0, \quad \dot{z}(0) = \dot{Z} \quad \text{with} \quad \dot{Z} > 0$$
$$\dot{x}(0) = \dot{X} \quad \text{and} \quad \dot{y}(0) = \dot{Y}.$$ (9)

The solution for z and $\dot{z}$ is easily obtained.

$$z(t) = \frac{\dot{Z}}{\Omega_{\perp}}\sin\Omega_{\perp}t + \frac{\dot{Y}}{\Omega_{\perp}}(1 - \cos\Omega_{\perp}t)$$ (10)

$$\dot{z}(t) = \dot{Z}\cos\Omega_{\perp}t + \dot{Y}\sin\Omega_{\perp}t.$$ (11)

It is independent of the initial x velocity, $\dot{X}$, since at $t = 0$, $B_{\perp}$ is in the x direction,
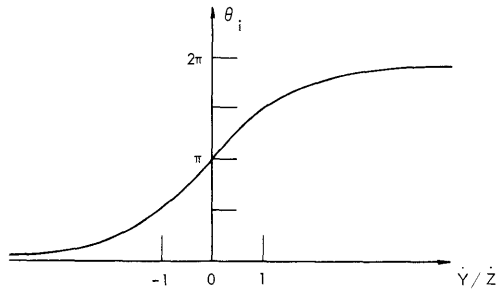
Fig. VIII-8.   Interaction angle vs initial velocity.

and the force from the cross product is only sensitive to $\dot{Y}$. If an ion spirals into $B_\perp$ at $z = 0$ such that $\dot{Y} = 0$, then superposed on the cyclotron motion at Ω_z in the perpendicular plane, it appears to orbit in the z direction at $\Omega_\perp$ and it reappears at $z = 0$ one-half cycle later with its z velocity turned around. This constitutes the reflection. In this case, the time t_i, or interaction angle $\theta_i = \Omega_\perp t_i$, during which the particle remains in the cavity is given by $\theta_i = \pi$. When $\dot{Y}$ is other than zero, θ_i can be determined by setting Eq. 10 equal to zero. The result is represented in Fig. VIII-8. Thus regardless of the initial velocity, the particle can always be reflected, provided that the field extends over the size of the orbit as given by Eq. 10.

Typical numbers that are feasible for a laboratory experiment are as follows:

$$\left.\begin{array}{l} 1 \text{ volt protons} \\ B_z = 1000 \text{ gauss} \end{array}\right\} \quad r_b \approx 1 \text{ mm}$$

$$\omega = |\Omega_z| \approx 10^7$$

$$\left.\begin{array}{l} B_\perp = 100 \text{ gauss} \\ \Omega_\perp \approx 10^6 \end{array}\right\} \quad r_z \approx 1 \text{ cm penetration}$$

Cavity dissipation ≈ 2 kw.

The similarity of this device with the magnetic "corkscrew"[4] should be noted. What the corkscrew does in space, the rotating fields do in time, and they have the advantage of being resonant for particles of all velocities.

D. R. Whitehouse

References

1. F. G. Insinger, H. J. Hopman, J. Kistemaker, J. Nuclear Energy, Part C, Vol. 5, page 223, 1963.

2. H. A. Blevin and P. C. Thonemann, Nuclear Fusion, Proceedings of the Salzburg Conference, 1962, Supplement Part I, p. 55.

3. P. W. Jameson, Electromagnetic compression, Quarterly Progress Report No. 72, Research Laboratory of Electronics, M. I. T., January 15, 1964, pp. 99-101.

4. R. C. Wingerson, Electron-beam trapping, Quarterly Progress Report No. 60, Research Laboratory of Electronics, M. I. T., January 15, 1961, pp. 59-65.

C. EFFECT OF GAS FLOW ON A SPIRAL INSTABILITY IN A PLASMA COLUMN

During the course of our studies of the influence of flow on the properties of the positive column in a glow discharge, spiral instability has been observed. Under ordinary

Fig. VIII-9.   Spiral instability brought to rest by gas flow in an argon plasma column.

conditions in a gas at rest, this instability is observed indirectly by the increase in the diffusion rate produced by the instability. In the presence of gas flow, however, we can readily bring the entire spiral to rest, study it visually, and investigate its geometrical properties as a function of the magnetic field and other parameters. A typical example of such a spiral instability in an argon discharge is shown in Fig. VIII-9. Qualitative observations concerning the influence of flow on the spiral radius and the spiral pitch have been made, and further detailed quantitative studies will be undertaken.

K. W. Gentle, K. U. Ingard, G. Bekefi

D. CYCLOTRON RADIATION OF A PLASMA GENERATED BY AN ELECTRON BEAM

We present results of measurements of the nonthermal microwave emission from a plasma generated by an electron beam fired into un-ionized mercury vapor. The beam and the plasma column are in a uniform magnetic field. In the experiments the plasma frequency of the beam, ω_{pb}, and the plasma frequency ω_{pp} of the secondary plasma itself are very much less than the microwave radian frequency ω ($\omega_{pb}^2/\omega^2 \lesssim 0.01$; $\omega_{pp}^2/\omega^2 \lesssim 0.1$). Under these conditions the emission spectrum is found to consist of a series of double lines, with each successive doublet positioned near a harmonic of the electron-cyclotron frequency $\omega = n\omega_b = (neB_o/m)$, $(n=1, 2, 3 \ldots)$. The two components of each doublet have markedly different behavior. One component (labelled I) is Doppler-shifted to a frequency that is higher or lower than that given by $\omega = n\omega_b$, the variation depending on whether the observations are made in the direction of the beam or in the opposing direction. Measurements are made at constant ω and varying ω_b. Thus a shift in frequency manifests itself as a shift in ω_b. The other component (II) of each doublet does not exhibit Doppler displacement; instead, it is displaced from $\omega = n\omega_b$ to a higher frequency by an amount that is proportional to the electron-beam density. The intensity of successive doublets decreases rapidly with increasing harmonic number n; nevertheless, the absolute magnitudes greatly exceed those expected from single-particle emission in a thermal plasma. When the mercury vapor is removed from the column and no secondary plasma forms, the only spectral line observed is a Doppler-shifted fundamental (n=1; component I). In this case the emission can be explained entirely on the basis of individual beam

electrons gyrating in the magnetic field.

In the experiments the electron beam is produced by a focused, magnetically shielded Pierce gun[1] with a perveance $i \times V^{-3/2} = 1 \times 10^{-6}$ amp-volt$^{-3/2}$. The electron beam has a diameter of 0.2 cm and traverses the axis of a quartz tube (100 cm in length, 2.5 cm in diameter) placed concentrically in a solenoid. The beam current is collected at the far end of the tube; in no case does the beam exceed 5 ma, and thus the maximum
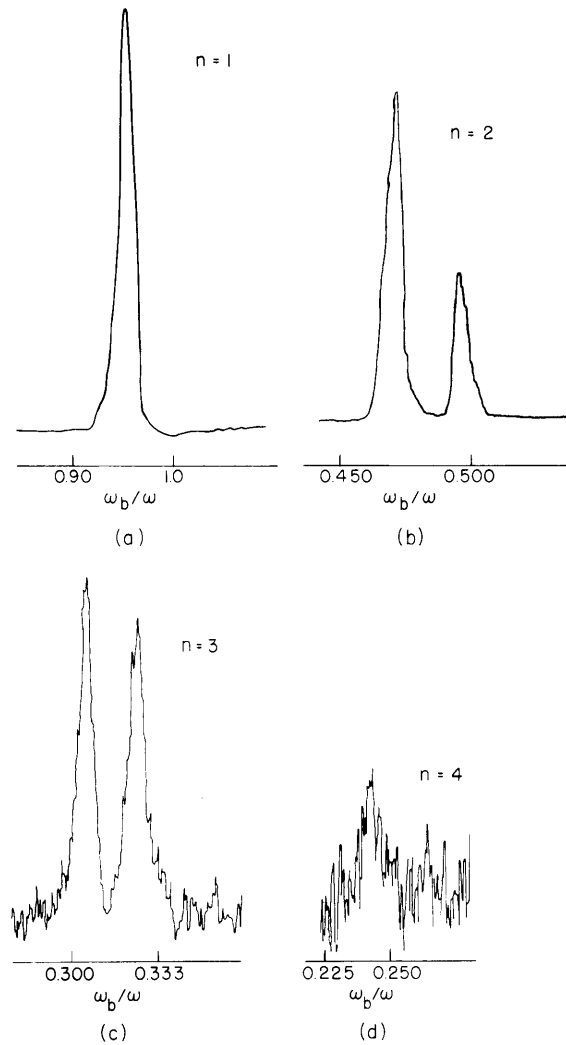

Fig. VIII-10. Radiation intensity viewed along the direction of the beam as a function of magnetic field, for the first four harmonics. Mercury vapor pressure, 1.8×10^{-4} mm Hg. (a) i = 3.0 ma, V = 210 volts; (b) i = 1.5 ma, V = 132 volts; (c) i = 3.1 ma, V = 270 volts; (d) i = 5 ma, V = 320 volts. The intensities of successive curves bear no relation to one another.

beam density is 1×10^9 cm^{-3}. As the beam enters the region of uniform axial magnetic field, it traverses a region of radial field and acquires transverse energy. Measurements show that approximately 15 per cent of the longitudinal beam energy supplied at the gun appears as electron energy at right angles to the axial magnetic field.

The vapor pressure of the mercury in the quartz column is maintained at the desired value by a constant-temperature bath. The experiments reported here refer only to a vapor pressure of 1.8×10^{-4} mm Hg. The beam and the faint halo of secondary plasma around it pass axially through a 50-cm long section of S-band waveguide, one end of which is terminated by a matched load, and the other connected to a radiometer[2] operated at a fixed frequency of 3000 Mc and a bandwidth of 2 Mc.

Figure VIII-10 shows plots of the radiation intensity as a function of magnetic field B for fields in the neighborhood of the first four harmonics. In each case the emission is observed in the direction of the electron-beam velocity. Figure VIII-10b and 10c exhibits the two components of the doublet referred to earlier. The Doppler-shifted component I lies nearer the value $\omega = n\omega_b$ than component II. Figure VIII-10a for the fundamental shows component II only; the less intense component I lies within the linewidth of component II. The fourth harmonic is weak, its linewidth is relatively large, and the Doppler-shifted component is not resolved.

Figure VIII-11 compares the forward and backward emissions for the doublets situated near n = 1 and n = 2; the upper traces refer to emission observed in the direction
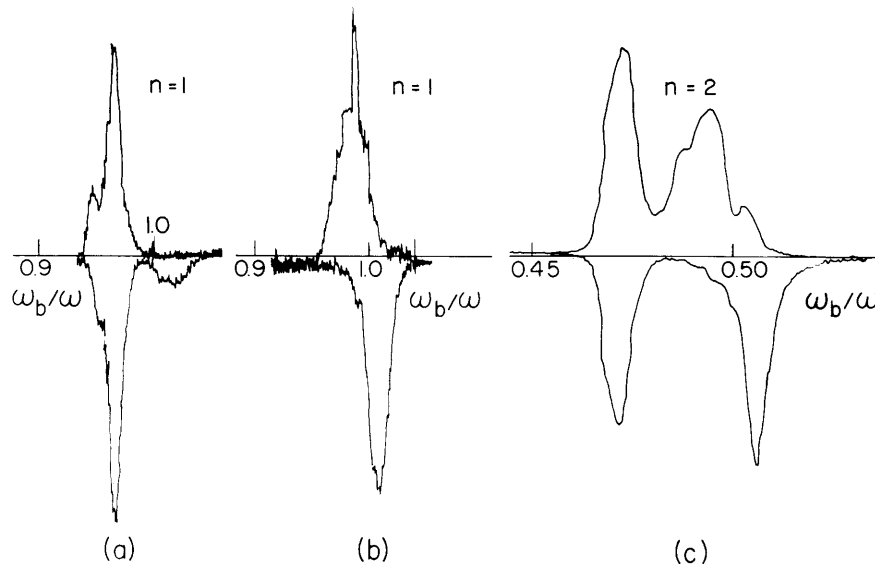

Fig. VIII-11.   Radiation intensity viewed along the direction of the beam (top trace) and in the opposing direction (bottom trace). (a) and (c) mercury vapor pressure, 1.8×10^{-4} mm Hg; (b) vapor pressure, $\approx 10^{-8}$ mm Hg.

of the electron beam and the inverted lower traces to emission in the opposite direction. Figure VIII-11a shows that the doublet is resolved if the emission is observed opposite to the beam velocity. Figure VIII-11b refers to the emission from the beam alone (the mercury vapor pressure is approximately 10^{-8} mm Hg); with no secondary plasma present, only the Doppler-shifted component I of the emission from the gyrating beam electrons is observed. The peak intensity of this emission is approximately 35 db below the emission in the corresponding Doppler-shifted component of Fig. VIII-11a. This illustrates the great enhancement in the emission of the beam electrons caused by the presence of the background plasma. Figure VIII-11c shows that component II is unaffected by changing the direction of observation.

Figure VIII-12 shows how the displacement Δf_b of the two components of a doublet varies with current i and voltage V of the electron beam. The parameter $2\pi\Delta f_b \equiv (e/m)|B-B_o|$, where B is the value of magnetic field at which the spectral line occurs for the fixed observation frequency ω, and $B_o = m\omega/ne$ is the magnetic field at which the
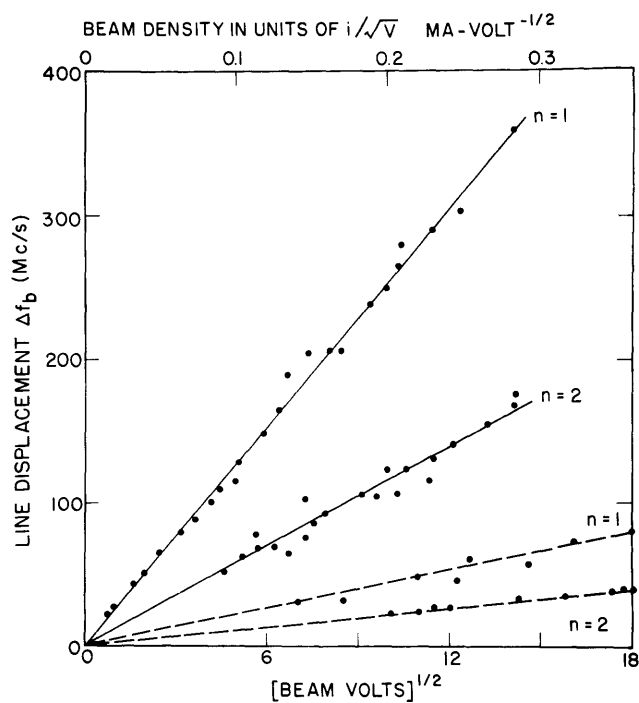

Fig. VIII-12. Line displacement Δf_b as a function of the electron-beam parameters. The two dashed curves show Δf_b of component I plotted as a function of $V^{1/2}$. The two solid curves show Δf_b of component II plotted as a function of beam density, $i \times V^{-1/2}$.

spectral line would occur ($\omega = n\omega_b$) in the absence of displacement. The two dashed curves of Fig. VIII-12 refer to the Doppler-shifted component I. This is compared with the familiar relation $\omega = n\omega_b + \vec{k} \cdot \vec{v}$, where $\vec{k}$ is the propagation vector of the wave and $\vec{v}$ the beam velocity. When the observation frequency ω is held constant and the magnetic field is varied, the shift Δf_b is given by $2\pi\Delta f_b = |k_\parallel v/n|$. The slope of the curves of Δf_b plotted as a function of $\sqrt{V}$ can now be used to determine $k_\parallel$; the value obtained is $2\pi/13.8$ cm^{-1}, which is equal to the propagation vector of the TE_{01} mode of the empty waveguide at the frequency of 3000 Mc. This means that the component of $\vec{k}$ parallel to the magnetic field is unaffected by the beam-plasma medium.

The two solid curves of Fig. VIII-12 show plots of Δf_b of component II as a function of $i \times V^{-1/2}$. Within the accuracy of the experiment, the straight-line relationship and the 2:1 ratio of slopes of the respective curves suggest that $\Delta f_b \propto \omega_{pb}^2/n$. This was verified by operating the electron gun first under space-charge-limited conditions, where V is varied and $i \times V^{-3/2}$ is constant, and then under temperature-limited conditions, where $i \times V^{-3/2}$ is not constant. Independent experiments[3] show that the constant of proportionality in the expression $\Delta f_b = (\text{constant} \times \omega_{pb}^2/n)$ is a function of the observation frequency ω.

Figure VIII-13 shows plots of the spectral line intensity (component II) of the first two harmonics as a function of beam density. The power in the fundamental is seen to be a steeply rising function of beam density with superimposed oscillations. Additional measurements show that the positions of the maxima and minima of the oscillations occur at definite values of V, independent of i. The power levels of the emitted radiation of the third and fourth harmonics (not shown) are approximately 10^{-15} and 10^{-16} watt, respectively.

The dashed lines of Fig. VIII-13 are plots of the total number of electrons Na^2 per unit length of plasma column, as a function of $i \times V^{-1/2}$ (N is the electron density in units of cm^{-3} and a is the effective radius of the plasma column). The upper curve refers to measurements at a magnetic field of 1000 gauss, the lower curve to measurements at 500 gauss. (The density of beam electrons alone is given by the relation $N_b a^2 = 3.4 \times 10^7 \times i \times V^{-1/2}$ ma-volt$^{-1/2}$.) Although the quantity Na^2 can be determined to an accuracy better than 20 per cent, a is not known except from visual observation of the column; a crude estimate gives a ~ 0.4 cm. We note that the plasma density increases gradually with increasing beam density and that therefore the oscillations in the emitted power observed as a function of ω_{pb} are not due to abrupt changes in plasma production.

Recent observations[4-8] of microwave emission and absorption by a variety of relatively cool steady-state and pulsed plasmas in a magnetic field have also shown harmonic emission. In those experiments the spectra consisted of a series of single lines of roughly equal intensity and width, positioned at or near the harmonics of the electron-cyclotron frequency; they were observed only when the plasma frequency was of the order
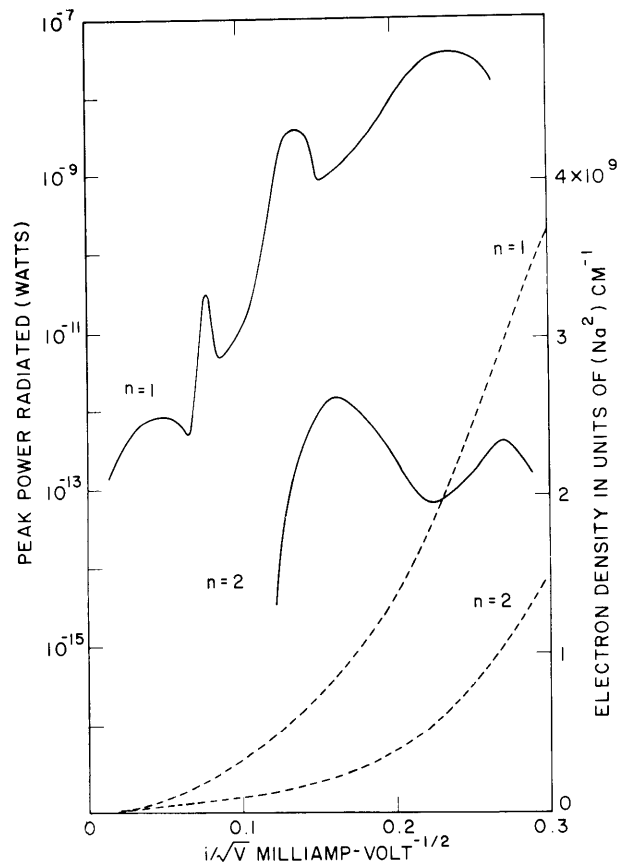
Fig. VIII-13. Peak power radiated in component II (solid curves)
and total electron density (dashed curves) as a
function of the electron-beam density. All meas-
urements shown are for space-charge saturated
operation, $i \times V^{-3/2} = 1 \times 10^{-6}$ amp-volt$^{-3/2}$. The
emitted power is that which flows down the wave-
guide within the frequency band of 2 mc.

of or greater than the microwave frequency ω. Just as in the present experiments, the
large harmonic emission (or absorption) could not be explained on the basis of single,
nonrelativistic electrons[9] gyrating in a uniform, infinite plasma with a Maxwellian dis-
tribution of particle velocities. Two alternate theoretical models[10,11] for finite plasma
geometry have been proposed recently, but it is not certain which of the two, if either,
pertains to the observed phenomena. In the first of these models, intense radiation
arises from excitation of plasma waves by fast, uncorrelated orbiting electrons. The
waves propagate within a cone whose axis is oriented at right angles to the magnetic
field; the waves are converted to electromagnetic waves at a plasma sheath. In the second
model harmonic emission results from uncorrelated electrons whose Larmor orbits
intersect physical walls or plasma sheaths.

The present experiments can be interpreted only on the basis of collective excitation of waves; they are not inconsistent with the model of Canobbio and Croci,[10] possibly modified to take into account coherence in the motion of the beam electrons.[12] There is no evidence, however, that harmonic emission caused by distortion of particle orbits[11] at sheaths plays a significant role in the present experiments. Experiments in which the electron beam is fired into ionized mercury vapor show that component II, but not component I, gradually disappears as the plasma density is increased. This suggests that the origin of component I is identical with that of the radiation reported.[4-8] See Section VIII-E.

G. Bekefi, E. B. Hooper, Jr.

References

1. J. R. Pierce, Theory and Design of Electron Beams (D. Van Nostrand Company, Inc., New York, 2d edition, 1954).

2. R. H. Dicke, Rev. Sci. Instr. 17, 268 (1946).

3. S. Gruber, W. D. McBee, and L. T. Shepherd, Private communication, 1964.

4. G. Landauer, Proceedings of the Fifth International Conference on Ionization Phenomena in Gases, Munich, 1961 (North-Holland Publishing Company, Amsterdam, 1962); J. Nuclear Energy, Part C, Vol. 4, p. 395, 1962.

5. G. Bekefi, J. D. Coccoli, E. B. Hooper, Jr., and S. J. Buchsbaum, Phys. Rev. Letters 9, 6 (1962).

6. H. Dreicer, Paper F3, Fifth Annual Meeting Division of Plasma Physics, San Diego, 1963.

7. C. D. Lustig, Paper F5, Fifth Annual Meeting Division of Plasma Physics, San Diego, 1963.

8. S. J. Buchsbaum, Paper I5, Fifth Annual Meeting Division of Plasma Physics, San Diego, 1963.

9. B. A. Trubnikov, Soviet Phys.-Doklady 3, 136 (1958).

10. E. Canobbio and R. Croci, Sixth International Conference on Ionization Phenomena in Gases, Paris, 1963.

11. A. Simon and M. N. Rosenbluth, Phys. Fluids 6, 1566 (1963).

12. W. P. Allis, S. J. Buchsbaum, and A. Bers, Waves in Anisotropic Plasmas (The M. I. T. Press, Cambridge, Massachusetts, 1963), Chapter 9.

E. CYCLOTRON RADIATION FROM AN ELECTRON BEAM IN A MERCURY DISCHARGE

The experiments reported here are a continuation of those reported by Bekefi and Hooper in Section VIII-D. The electron beam is now fired into a mercury discharge rather than into un-ionized mercury vapor, and the radiation measured as both beam and discharge currents are varied.

The electron beam is fired through a hole drilled in the discharge anode. In the pre-vious set of experiments there was no discharge in the tube. The discharge cathode at the far end was biased slightly positive and acted simply as a collector for the electron beam. In the present set of experiments the cathode had to be biased negative so that a discharge could be struck. The lack of positive bias on the discharge cathode pre-vented most of the beam electrons from being collected. To check the continuity between the previous set of experiments and the present set, the radiation was measured as the beam current was varied in the absence of a discharge, but with the discharge cathode grounded. The frequency shift vs the square root of the beam voltage is shown in Fig. VIII-14. It can be seen that component I behaves as a Doppler-shifted peak only at high beam currents when probably most of the beam is collected. In this region of beam currents, it was also found that Δf_b for component II was roughly proportional to $i/\sqrt{V}$,
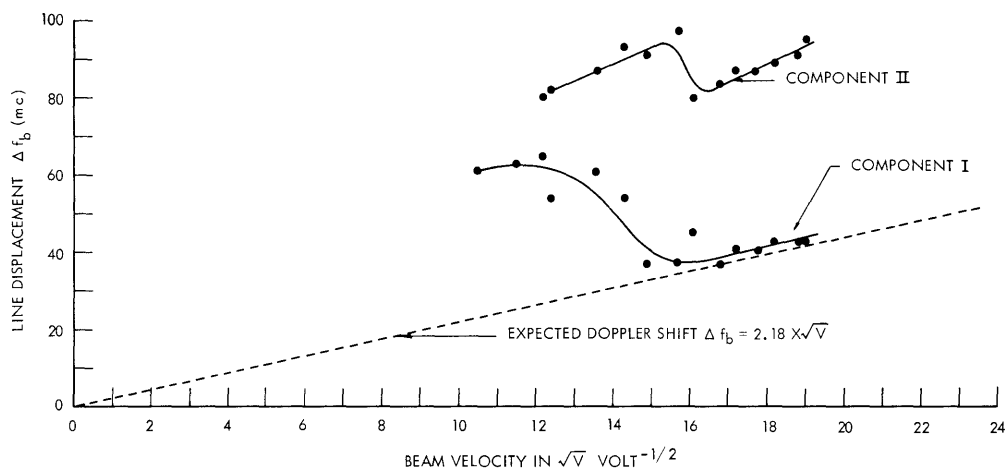

Fig. VIII-14. Line displacement Δf_b for the second harmonic as a function of $V^{1/2}$ with no discharge.

as in the previous experiments, although the slope is different. Thus we have approxi-mate agreement between the old experiments and the present set only at high beam cur-rents. We would expect the agreement to be worse when the discharge is actually turned on, since the cathode is biased negative, and even fewer of the beam electrons are col-lected.

As a consequence of the lack of positive bias on the discharge cathode, two parame-ters in the earlier set of experiments, $\sqrt{V}$, which was proportional to the velocity of the beam electrons, and $i/\sqrt{V}$, which was proportional to the density of the beam electrons, are no longer very meaningful parameters. Some electrons charge up the end walls of the tube and produce regions of space charge which reflect most of the beam electrons

back along the axis of the tube. The velocity of the beam electrons then varies along the axis and is no longer given solely by the accelerating beam voltage but should be considerably less than that. Some of the data (see discussion of Figs. VIII-14 and VIII-19) seems to indicate beam velocities much greater than that given by $\sqrt{V}$, but this is unreasonable, since the space-charge regions produce a retarding rather than an accelerating potential. The beam density will also be expected to vary along the axis of the tube and will not be simply given by $i/\sqrt{V}$.

Electron-density measurements were made by using a microwave cavity and are plotted in Fig. VIII-15. Density Na^2 is given in electrons per unit length, and the actual density is known only approximately by making a visual estimate of the radius a of the plasma column. It is seen that Na^2 is directly proportional to discharge current i_d and
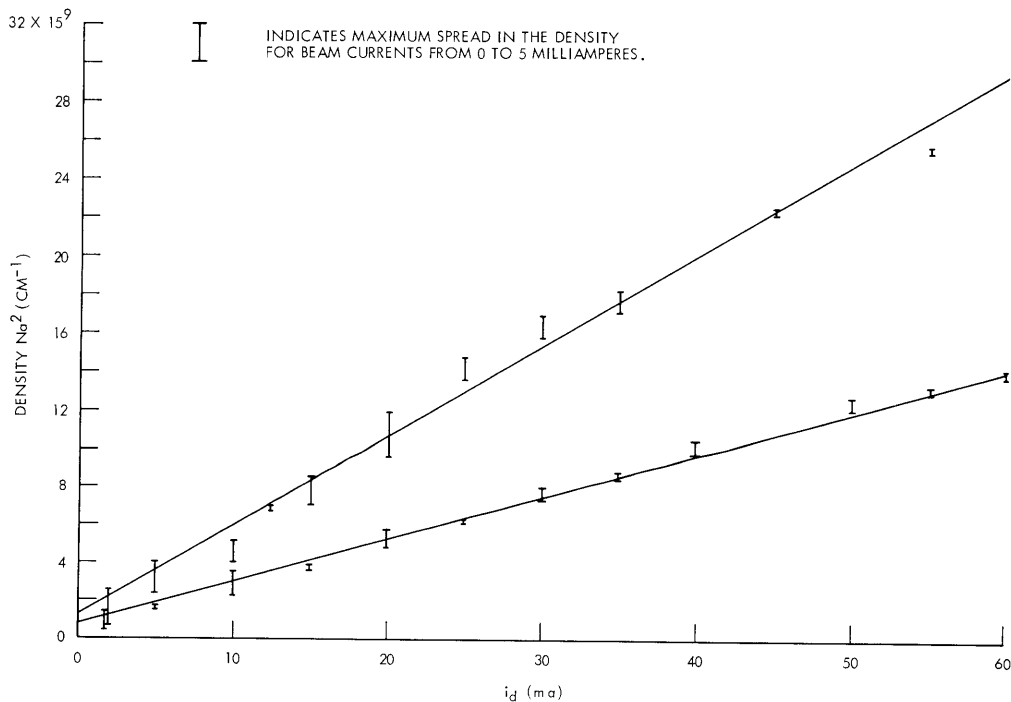

Fig. VIII-15. Electron density in units of (Na^2) cm^{-1} as a function of discharge current i_d.

the magnetic field B, and it is independent of the discharge voltage, beam current, and beam voltage.

Since the discharge current is proportional to Na^2, it is a convenient parameter against which to plot intensities and frequency shifts. A plot against i_d is equivalently a plot against electrons per unit length.

When the beam current is held constant and the discharge current is increased, component II decreases in intensity and disappears. The intensity of component I increases rapidly at low discharge currents, rises to a maximum, decreases, and goes through a minimum and another maximum. (See Fig. VIII-16.) The shapes of the curves for different beam currents are all similar, but as i_b is increased, the entire curve shifts
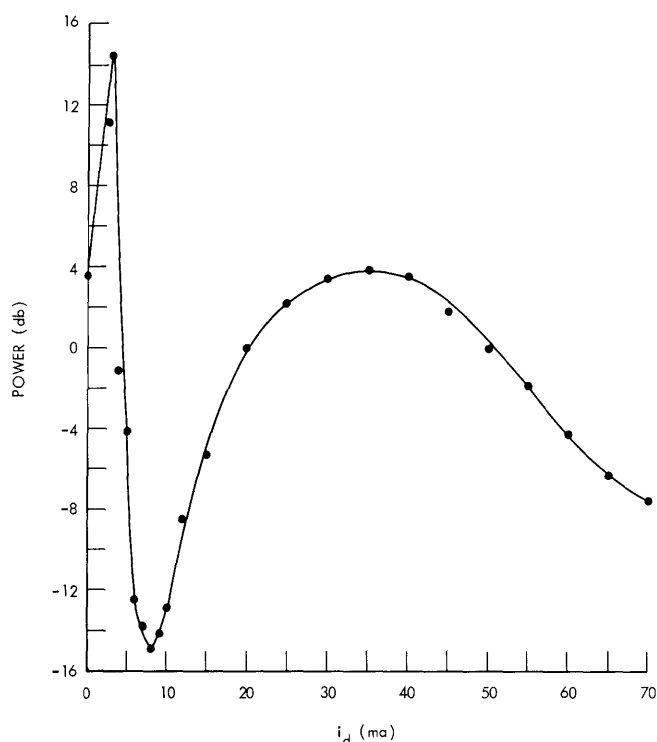

Fig. VIII-16. Radiation intensity of component I (second harmonic) in db above a standard noise source at 18510°K as a function of discharge current i_d with a beam current of 5. 0 ma.

upward in intensity and the positions of the maxima and minima shift to slightly higher values of i_d.

Figures VIII-17 and VIII-18 show plots of peak intensity vs beam current. The curves are generally monotonic upward in contrast to Fig. VIII-13 (Section VIII-D) even in the absence of a discharge. The results are different in the present experiments because the discharge cathode is not biased positive to collect all of the beam electrons.

Figure VIII-19 shows the frequency shift of component I plotted against discharge current. With no discharge (i_d=0) the shift agrees quite well with the Doppler shift corresponding to the actual beam voltage of 268 volts. When the discharge is turned on, Δf_b increases sharply and then gradually decreases with i_d, leveling off for high
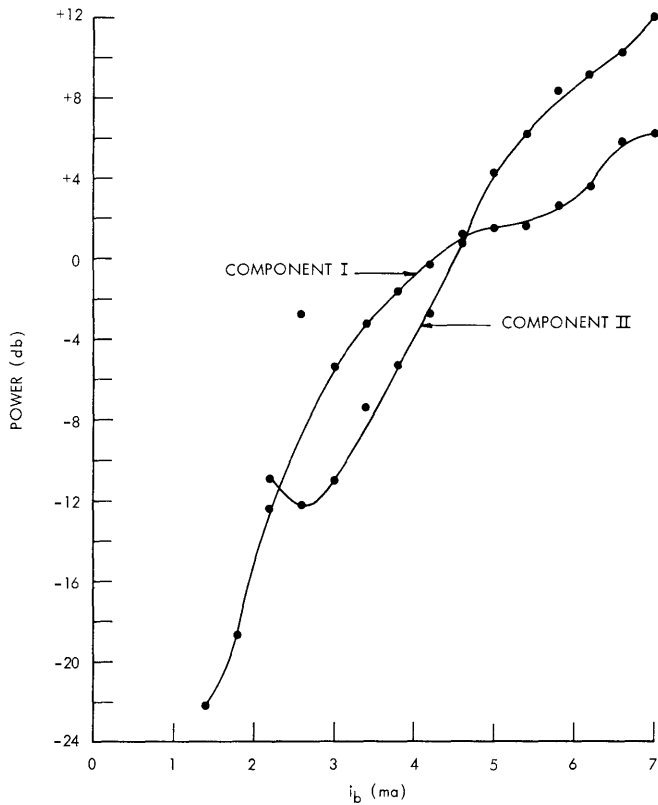
Fig. VIII-17.

Radiation intensity of the second harmonic in db above a standard noise source at 18510°K as a function of beam current i_b with no discharge.
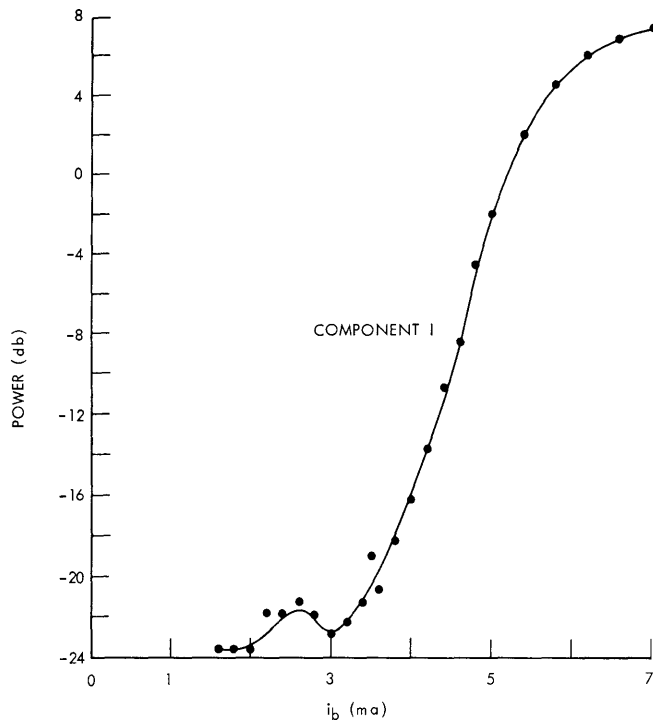

Fig. VIII-18.

Radiation intensity of component I (second harmonic) in db above a standard noise source at 18510°K as a function of beam current i_b with a discharge current of 60.0 ma.
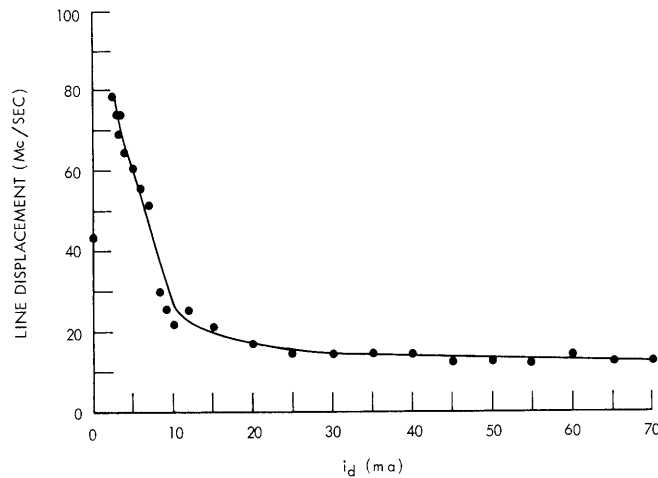
Fig. VIII-19. Line displacement Δf_b of component I (second harmonic) as a function of discharge current i_d with a beam current of 5. 0 ma.

discharge currents to a value equal to a Doppler shift corresponding to a beam accelerating voltage of only 33 volts. This high-current limit is reasonable, since the space-charge regions in the tube produce a retarding potential thereby slowing down the electrons and reducing the Doppler shift. The shifts at very low discharge currents cannot be explained in terms of this retarding potential. The shifts are equal to Doppler shifts corresponding to velocities much greater than that acquired in the gun. An explanation is found in the shift of the center of gravity of the Doppler line. Whenever observations were made in both forward and backward directions, the Doppler shift was always found to be less than that corresponding to the value of V_b. The center of gravity of the line, however, was shifted to higher frequencies. Thus the apparent Doppler shift was larger than that corresponding to V. This shift in the center of gravity of the Doppler line could be explained by an increase in the magnetic field when the discharge was turned on. Then the apparent field ω_b corresponding to the measured current through the magnet would be less than the actual field inside the magnet, and the parameter ω_b/ω would be less, which would be interpreted as an upward shift in frequency of any radiation peak. It is difficult to see how the discharge itself could have such an effective paramagnetic effect, since the effect is greatest when the discharge is weakest and decreases as i_d increases. It is thought that this is rather an instrumental effect, but its nature is not known.

Referring to Fig. VIII-14 we also see very large apparent Doppler shifts. The dashed line is the Doppler shift corresponding to the velocity acquired in the accelerating beam voltage. We sould expect all points of component I to lie on or under this line, since the space-charge regions should tend to decrease the beam velocity. It is

seen, however, that for small beam currents the points lie well above the line. We interpret this as a shift in the center of gravity of the line as was observed in the presence of a discharge rather than a large Doppler shift. Thus the anomalous behavior discussed above occurs even in the absence of a discharge.

R. L. Kronquist, E. B. Hooper, Jr., G. Bekefi